materials

MDPI

Article

First-Principles Study of Vacancies in Ti_3SiC_2 and Ti_3AlC_2

Hui Wang [1], Han Han [2,*], Gen Yin [3], Chang-Ying Wang [2], Yu-Yang Hou [1], Jun Tang [1], Jian-Xing Dai [2], Cui-Lan Ren [2], Wei Zhang [2] and Ping Huai [2,*]

1 School of Physics and Engineering, Henan University of Science and Technology, Luoyang 471003, China; nkxirainbow@gmail.com (H.W.); hyy9539@163.com (Y.-Y.H.); Tangjunguyue@126.com (J.T.)

2 Shanghai Institute of Applied Physics, Chinese Academy of Sciences, Shanghai 201800, China; wangchangying@sinap.ac.cn (C.-Y.W.); daijianxing@sinap.ac.cn (J.-X.D.); rencuilan@sinap.ac.cn (C.-L.R.); zhangwei@sinap.ac.cn (W.Z.)

3 Department of Electrical Engineering, University of California, Los Angeles, CA 90095, USA; genyin@ucla.edu

* Correspondence: hanhanfudan@gmail.com (H.H.); huaiping@sinap.ac.cn (P.H.); Tel.: +86-21-3351-2449 (H.H.); +86-21-3351-4793 (P.H.); Fax: +86-21-3351-4060 (H.H. & P.H.)

Academic Editor: Duncan H. Gregory

Received: 23 December 2016; Accepted: 23 January 2017; Published: 25 January 2017

Abstract: MAX phase materials have attracted increased attention due to their unique combination of ceramic and metallic properties. In this study, the properties of vacancies in Ti_3AlC_2 and Ti_3SiC_2, which are two of the most widely studied MAX phases, were investigated using first-principles calculations. Our calculations indicate that the stabilities of vacancies in Ti_3SiC_2 and Ti_3AlC_2 differ greatly from those previously reported for Cr_2AlC. The order of the formation energies of vacancies is $V_{Ti(a)} > V_{Ti(b)} > V_C > V_A$ for both Ti_3SiC_2 and Ti_3AlC_2. Although the diffusion barriers for Ti_3SiC_2 and Ti_3AlC_2 are similar (~0.95 eV), the properties of their vacancies are significantly different. Our results show that the vacancy–vacancy interaction is attractive in Ti_3AlC_2 but repulsive in Ti_3SiC_2. The introduction of V_{Ti} and V_C vacancies results in the lattice constant *c* along the [0001] direction increasing for both Ti_3SiC_2 and Ti_3AlC_2. In contrast, the lattice constant *c* decreases significantly when V_A are introduced. The different effect of V_A on the lattice constants is explained by enhanced interactions of nearby Ti layers.

Keywords: MAX phases; vacancies; diffusion barrier; density functional theory

1. Introduction

The MAX phases form a large family of ternary carbides/nitrides with the general formula Mn+1AXn, where n varies from 1 to 3, M is an early transition metal, A is an A-group element, and X is C or N [1–3]. The MAX phases have a unique combination of the properties of ceramics and metals. Similar to metals, they are electrically and thermally conductive, easy to machine, ductile at high temperatures, and exceptionally resistant to damage and thermal shock. Like ceramics, they are elastically rigid, lightweight, and oxidation resistant.

Titanium aluminum carbide (Ti_3AlC_2) and titanium silicon carbide (Ti_3SiC_2) are 312 MAX phases. Like most MAX phases, Ti_3SiC_2 is stiff (Young's modulus 352 GPa [4], tough (toughness 9 MPa $m^{1/2}$ [5]), thermally conductive (37 $W \cdot m^{-1} \cdot K^{-1}$ [6]), and electrically conductive (4.5×10^6 $\Omega^{-1} \cdot m^{-1}$ [7]). The properties of Ti_3AlC_2 differ slightly from those of Ti_3SiC_2; for example, it has a lower Young's modulus (297 GPa) and electrical conductivity (2.9×10^6 $\Omega^{-1} \cdot m^{-1}$). Both materials are readily machinable and tolerant to damage and thermal shock [8]. Ti_3SiC_2, has two polymorphs, i.e., α and β phases [9]. α-Ti_3SiC_2 has the same structure as Ti_3AlC_2, but the Si layer in β-Ti_3SiC_2

is shifted. β-Ti_3SiC_2 is a metastable phase, therefore α-Ti_3SiC_2 has been more widely studied [8,10]. For simplicity, only α-Ti_3SiC_2 is considered in this work.

On one hand, defects can be unintentionally introduced into Ti_3SiC_2 and Ti_3AlC_2 during their synthesis. These materials are refractory ceramics and considerable concentrations of vacancies and impurities are introduced during their multi-component nanolaminate formation. On the other hand, Ti_3SiC_2 and Ti_3AlC_2 are potential structural materials for nuclear applications. Defects are created in the lattices of Ti_3SiC_2 and Ti_3AlC_2 by irradiation when the incident particles displace atoms from their substitutional positions. As mentioned above, their unique properties make Ti_3SiC_2 and Ti_3AlC_2 suitable candidates to be adopted in applications where materials are subject to extreme environments, such as nuclear reactors [11–14]. Amorphization is an important factor to evaluate the irradiation-resistant of a material. The resistance of amorphization is dependent on the competing effects between the defect production and annihilation rate. Vacancies are the simplest defects in MAX phases. A deeper knowledge of the properties of them in Ti_3SiC_2 and Ti_3AlC_2 is crucial for the understanding of the defect production, annihilation process, and phase stability [15–23].

A large number of experimental studies [11–14,24–31] have investigated the properties of Ti_3SiC_2 and Ti_3AlC_2 when subjected to irradiation with heavy ions and neutrons. Nappé et al. [11] studied the defect properties of Ti_3SiC_2 under Au-, Kr-, and Xe-ion irradiation. They observed generation of many defects in the structure and an expansion along the *c* axis. Liu et al. [12] reported that atomic disorder appeared in $Ti_3(Si,Al)C_2$ after Kr-ion irradiation, but the typical layered structure was preserved. Whittle et al. [13] reported that Ti_3AlC_2 and Ti_3SiC_2 showed high tolerance to damage from Xe-ion irradiation. Hoffman et al. [14] compared the neutron irradiation tolerances of Ti_3SiC_2 and Ti_3AlC_2 with those of SiC and alloy 617. They concluded that Ti_3SiC_2 and Ti_3AlC_2 have good irradiation tolerances.

Compared with experimental methods, first-principles calculations have the advantage of enabling the study of materials at the atomic scale. Such calculations have frequently been used to predict the crystal structures and stabilities of MAX phases, and to model their defects and related properties. Wang et al. [15–17] systematically studied the effects of vacancies and impurities in the Ti_2AlC phase. They calculated the stabilities of Ti_2AlC samples with different types of vacancies. Music et al. [18] studied the vacancies in Ti_4AlN_3, and reported that the introduction of about 25% N vacancies in Ti_4AlN_3 is energetically favorable. Tan et al. [19] studied vacancy diffusion in Ti_2AlC and its impurity phase Ti_3AlC. Du et al. [20] studied the C vacancies in Ta_4AlC_3, and suggested that the introducing of C vacancies decreases the phase stability. Han et al. [21] studied defect stabilities in Cr_2AlC under different magnetic orderings.

However, although Ti_3SiC_2 and Ti_3AlC_2 are the most extensively studied MAX phases experimentally, theoretical investigations of their defect properties are rare. Medvedev at al. [22] studied the influence of disorder associated with the presence of vacancies on the electronic properties of Ti_3SiC_2. They found that the presence of C vacancies in Ti_3SiC_2 caused local perturbations of the electronic structures. Zhao et al. [23] studied the formation energies of different defects in Ti_3SiC_2 and Ti_3AlC_2. They found that replacement of Ti by Al in Ti_3AlC_2 was more energetically favorable than replacement of Ti by Si in Ti_3SiC_2. These previous theoretical works mainly investigated point defect stabilities. In this work, we focus on the formation, stability, geometry, and diffusion properties of vacancies in Ti_3SiC_2 and Ti_3AlC_2.

2. Theoretical Method

Our calculations were performed under the framework of density functional theory as implemented in the Vienna ab initio simulation package (VASP) [32,33]. The projected augmented wave method (PAW) [34] and the generalized gradient approximation (GGA) [35] were used. According to our previous study on MAX phases [19,21], the exchange and correlation energies were calculated using the Perdew−Burke−Ernzerhof (PBE) functional [36]. The wave functions were expanded in a plane-wave basis set with an energy cutoff of 400 eV. The lattice constants and internal freedom

of the unit cell were fully optimized until the Hellman-Feynman forces on the atoms were less than 0.01 eV/Å. The effective charge for each atom (charge difference after bonding) is given using Bader charge analysis [37].

In order to simulate a single vacancy structure, we employed a 2 × 2 × 1 supercell, which contains 48 atoms. According to our previous studies on defects properties of MAX phases [19,21,38], the supercell has been proved to be sufficient to reproduce the defect structures. The special k-point sampling integration was used over the Brillouin zone by using the Γ-centered 5 × 5 × 5 for this supercell [39]. All these calculation setups were checked using a larger energy cutoff and k-mesh; the results of total energy and Hellmann-Feynman forces are convergent within 0.01 eV and 0.01 eV/Å, respectively.

To evaluate the energy barrier of an Al-vacancy, the climbing image nudged elastic band method (cNEB) [40,41] was employed to investigate the saddle points and minimum energy paths for vacancy diffusion from the initial state to the final state. In all transition state search calculations performed in this paper, a total of eight images were used (not including the initial and final images of each transition).

3. Results and Discussion

3.1. Properties of Perfect Ti_3SiC_2 and Ti_3AlC_2

Ti_3SiC_2 and Ti_3AlC_2 are both belonging to 312 phases with the same crystal symmetries, as shown in Figure 1. They are based on layers of hexagonally close-packed Ti and Al/Si layers with C occupying octahedral centers between the Ti layers. The structures of Ti_3SiC_2 and Ti_3AlC_2 can also be regarded as alternating stacks of two layers of edge-sharing Ti_6C octahedra and a planar close-packed Al/Si layer. The Si/Al atoms are located in the Wyckoff 2*b* (0, 0, 1/4) positions and the C atoms are in *4f* (1/3, 2/3, z_C) positions. There are two types of non-equivalent Ti atoms, denoted by Ti(a) and Ti(b), which are located at 4*f* (1/3, 2/3, z_{Ti}) and 2*a* (0, 0, 0), respectively. The calculated structural parameters for Ti_3SiC_2 and Ti_3AlC_2 are listed in Table 1; the experimental results are also listed for comparison. The differences between the calculated and experimental values of the lattice constants are all smaller than 1%, indicating reliable predictions by our PBE calculations.

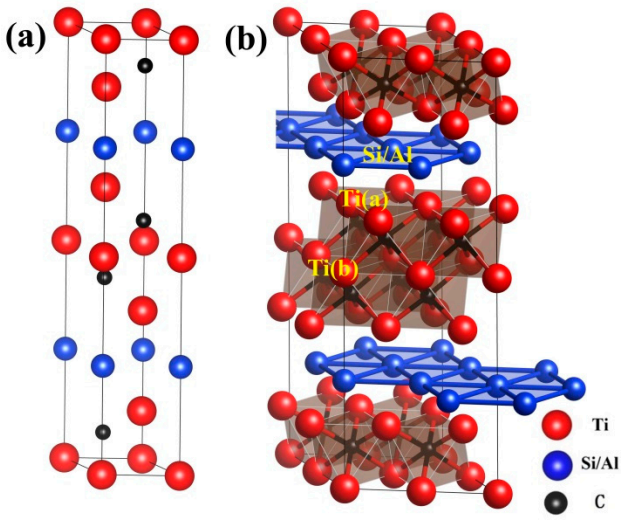

Figure 1. Crystal structures of Ti_3SiC_2 and Ti_3AlC_2: (**a**) conventional cell and (**b**) supercell used to model defect configurations. Red, blue, and black balls represent Ti, Si/Al, and C atoms, respectively. Two types of non-equivalent Ti atoms are identified.

Table 1. Calculated (Cal.) lattice constants a and c (Å), c/a ratio, and internal structural parameters z_{Ti} and z_C for Ti_3SiC_2 and Ti_3AlC_2. Experimental values (Exp.) are also listed.

Material	Method	a (Å)	c (Å)	c/a	z_{Ti}	z_C
Ti_3SiC_2	Cal.	3.075	17.734	5.767	0.135	0.572
	Exp. [42]	3.07	17.67	5.76	0.135	0.568
Ti_3AlC_2	Cal.	3.082	18.642	0.648	0.127	0.569
	Exp. [6]	3.075	18.578	0.641	0.128	0.564

After optimization of the crystal structures, the mechanical property parameters were calculated. In the Voigt–Reuss–Hill approximation [43–45], the bulk modulus B, and the shear modulus G are the average of the values obtained by Voigt and Reuss approximations [43]. The Young's modulus (E), the Poisson ratio (v), the transverse (V_t), longitudinal (V_l), and average (V_a) acoustic wave velocities, and the Debye temperature (Θ_D) can be obtained. Experimental values for Ti_3AlC_2 have not been reported, therefore only the calculated values for Ti_3SiC_2 are listed in Table 2 and compared with the experimental values. The results show that the calculated values are reasonably consistent with the experimental results.

Table 2. Calculated elastic properties of Ti_3SiC_2, including the bulk modulus B, the shear modulus G, the Young's modulus E, the Poisson ration v, the acoustic wave velocities (V_l, V_t, V_a), and the Debye temperature Θ_D. The experimental values [46] are also listed for comparison.

Properties	B (GPa)	G (GPa)	E (GPa)	v
Cal.	200.3	132.3	325.2	0.23
Exp.	187	142	339	0.2
Properties	V_l **(Km/s)**	V_t **(Km/s)**	V_a **(Km/s)**	Θ_D **(K)**
Cal.	9.17	5.43	6.0	780
Exp.	9.14	5.61	6.2	804

3.2. Formation Energies of Vacancies in Ti_3SiC_2 and Ti_3AlC_2

The stabilities of vacancies at different atomic sites in crystals can be evaluated by the vacancy formation energy, which is defined as follows:

$$E_{vac}(V_X) = E_{tot}(V_X) - E_{tot}(perf) + \mu_X, \quad (1)$$

where $E_{vac}(V_X)$ is the vacancy formation energy of atom X (X = Ti, Al, C), $E_{tot}(V_X)$ is the calculated total energy of a cell with defect X, $E_{tot}(perf)$ is the total energy of a perfect crystal without defects, and μ_X is the chemical potential of X. Here, μ_X is chosen as the energy of an isolated X atom for simplicity.

As shown in Figure 2, for both Ti_3SiC_2 and Ti_3AlC_2, A-group element vacancies have the lowest formation energies, indicating that they are easily formed. The non-equivalent Ti(a) and Ti(b) atoms have different vacancy formation energies. Figure 1 shows that the Ti(a) atoms are located between Al and C layers. Ti(a) forms covalent bonds with C atoms, but forms weak metallic bonds with Al atoms. In contrast, the Ti(b) atoms are located at the center of [Ti_6C] octahedra, and have stronger interactions with surrounding atoms. The vacancy formation energies of the Ti(b) atoms are therefore larger than those of the Ti(a) atoms. The order of the vacancy formation energies is $V_{Ti(a)} > V_{Ti(b)} > V_C > V_A$. These results for Ti_3SiC_2 and Ti_3AlC_2 differ greatly from our previously reported results for Cr_2AlC, in which the Al vacancies were predicted to have high formation energies and the Cr vacancies were predicted to have low formation energies [21]. The formation energy of V_{Al} is 0.9 eV lower than that of V_{Si}, indicating that an A-group element mono-vacancy is more easily formed in Ti_3AlC_2.

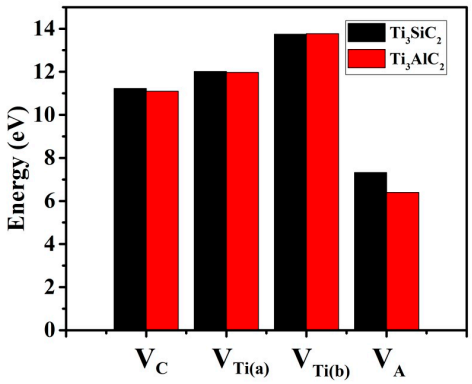

Figure 2. Vacancy formation energies (E_{vac}, eV) of V_C, $V_{Ti(a)}$, $V_{Ti(b)}$, and V_A (V_{Si}/V_{Al}) in Ti_3SiC_2 and Ti_3AlC_2.

3.3. Vacancy–Vacancy Interactions of V_A

These above calculation results indicate that V_A vacancies are easily formed when Ti_3SiC_2 and Ti_3AlC_2 are in oxidizing, corrosive, and irradiation environments. The effects of V_A vacancies on the phase stabilities of Ti_3SiC_2 and Ti_3AlC_2 were explored by introducing more vacancies and calculating their vacancy formation energies:

$$E_{vac}(V_X) = E_{tot}(V_X) - E_{tot}(\text{perf}) + \mu_X, \quad (2)$$

where n is the concentration of V_A vacancies in Ti_3SiC_2 and Ti_3AlC_2. Figure 3 shows that for Ti_3AlC_2 the vacancy formation energy decreases as the number of vacancies increases, indicating that existing vacancies can accelerate the formation of new vacancies. Therefore, decomposition of Ti_3AlC_2 can be caused by formation of a large number of vacancies in the Al layers. In contrast, the relationship between the V_A content and the vacancy formation energy is different for Ti_3SiC_2; the vacancy formation energy increases significantly with the increasing number of vacancies. This indicates that it is difficult to introduce a new V_{Si} near the original one because of the increased vacancy formation energy. Based on these results, it is reasonable to conclude that the interactions between nearby vacancies in Ti_3AlC_2 are attractive, but are repulsive in Ti_3SiC_2. The vacancies therefore tend to disperse in Ti_3SiC_2 but are accommodated in Ti_3AlC_2.

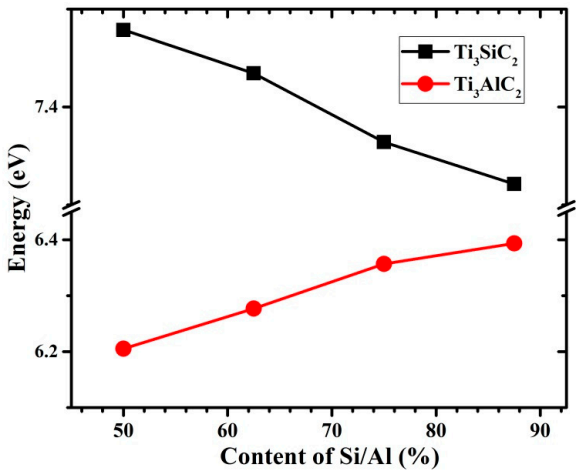

Figure 3. Vacancy formation energy (E_{vac}, eV) of V_A (V_{Si}/V_{Al}) dependences on A-group element atomic content of Ti_3SiC_2 and Ti_3AlC_2.

In order to verify this conclusion, we calculated and compared the vacancy formation energies for three configurations with two vacancies introduced at different locations. The results are shown in Figure 4. For Ti_3SiC_2, the configuration with two vacancies located in different layers has a low formation energy. Vacancy pair formation (config.1) increases the energy by ~0.2 eV compared with the other two configurations (config.2 and config.3). In contrast, config.1 is energetically more favorable for Ti_3AlC_2. Therefore, Ti_3SiC_2 should be more stable than Ti_3AlC_2 in a corrosive environment.

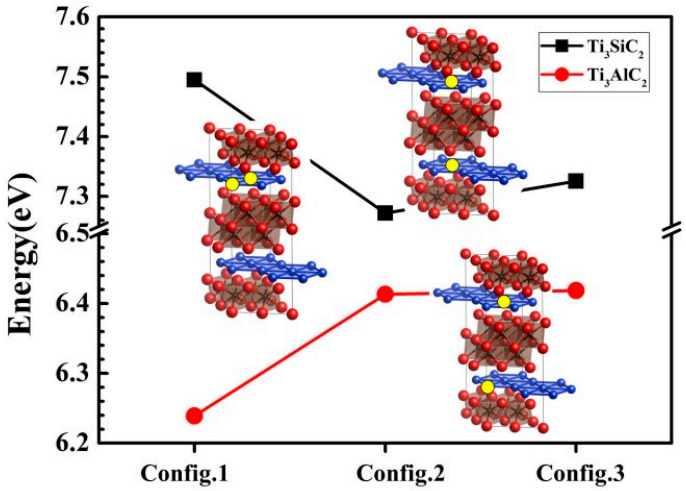

Figure 4. Vacancy formation energies (E_{vac}, eV) for V_A (V_{Si}/V_{Al}) in three defect configurations of Ti_3SiC_2 and Ti_3AlC_2. Yellow circles represent vacancies in Si/Al layers.

3.4. Diffusion of V_A Vacancies

It is well known that the Al/Si atoms move in MAX phases predominantly by vacancy-mediated diffusion [19,21]. To ensure that the supercell was sufficiently large to avoid the influence of adjacent cells, a $\sqrt{3} \times 2\sqrt{3} \times 1$ supercell was used to calculate the diffusion barrier. The obtained values are consistent with those obtained using a $2 \times 2 \times 1$ supercell.

The calculated diffusion barriers (B_{diff}) for Si/Al in Ti_3SiC_2 and Ti_3AlC_2 are less than 1 eV; these are close to the self-diffusion barriers of many metals, as shown in Table 3. The diffusion of vacancies along the (0001) plane can therefore occur frequently in these two materials. As mentioned previously, the interactions of vacancies in Ti_3SiC_2 are repulsive, whereas they are attractive in Ti_3AlC_2. A new vacancy will therefore diffuse away from an existing vacancy in Ti_3SiC_2; this does not greatly affect the stability of the material. In contrast, the low diffusion barrier indicates that vacancies in Ti_3AlC_2 tend to be accommodated. A large number of vacancies may therefore lead to decomposition of the material. The diffusion of atoms in the corresponding free-standing Si/Al layers was also studied using the same method shown in Figure 5. The diffusion barriers in free-standing layers (~0.2 eV) are clearly different from those in the Si/Al layers of MAX phases (~0.95 eV). These results indicate that the main contribution to the barrier is the interaction between the Al/Si and Ti layers, rather than the interaction in the Si/Al layers.

Table 3. Diffusion barriers for V_A in Ti_3SiC_2 and Ti_3AlC_2. Self-diffusion barriers of Al, C, and Ni are also listed for comparison.

Material	Ti_3SiC_2/Ti_3AlC	Cu	Al	Ni
Barrier (eV)	0.95	0.92 [47]	0.61 [48]	1.4–1.8 [49,50]

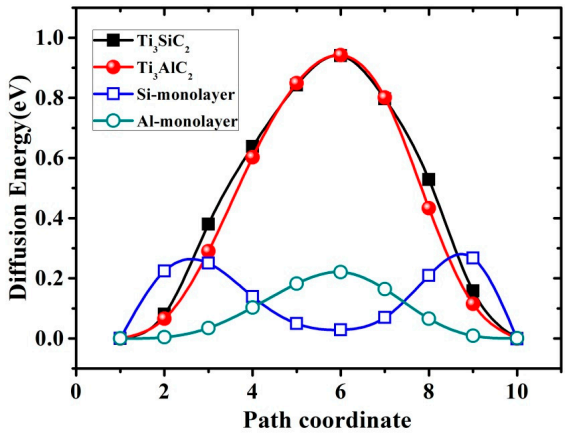

Figure 5. Calculated energy plots for diffusion of Si/Al vacancy in Ti_3SiC_2 and Ti_3AlC_2 using cNEB method. Energy barriers (B_{diff}) for Ti_3SiC_2 and Ti_3AlC_2 are both 0.95 eV. Empty squares/circles denote energies for Si/Al vacancy diffusion in free-standing Si/Al layers; these indicate a low barrier of ~0.2 eV.

3.5. Effects of Vacancies on Lattice Constants

Defects in a material can lead to changes in the lattice constants. For example, irradiation of nuclear graphite increases the lattice constant *c* along the [0001] direction, and decreases the lattice constants *a* and *b* in the (0001) plane. This is because of the large numbers of interstitial carbons in the graphite interlayers. In this work, the effects of vacancies on the lattice constants of Ti_3SiC_2 and Ti_3AlC_2 were investigated. Figure 6 shows the trends in the changes in the lattice constants of Ti_3SiC_2 and Ti_3AlC_2 with increasing the number of vacancies in the supercell. The introduction of vacancies increases the lattice constant *a* and decreases *c*. The change in *a* is negligible, but a significant change in *c* is observed along the [0001] direction. The lattice constant changes for Ti_3SiC_2 are larger than those for Ti_3AlC_2.

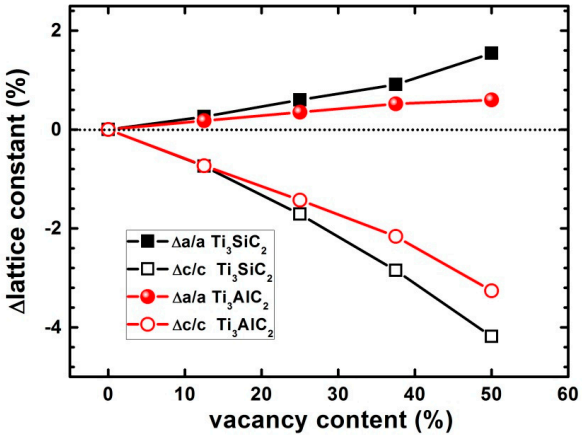

Figure 6. Changes in lattice constants of Ti_3SiC_2 and Ti_3AlC_2 with respect to concentration of Si/Al vacancies. Black and red lines indicate results for Ti_3SiC_2 and Ti_3AlC_2, respectively.

The lattice constant changes induced by other types of vacancies were also calculated. The results for V_{Ti} and V_C are the opposite of those for V_A. As shown in Figure 7, when V_{Ti} and V_C vacancies are introduced, the lattice constant *a* decreases and *c* increases. The effects of V_A and V_{Ti}/V_C on the lattice constants differ because the interactions between the corresponding atoms and their surrounding atoms are different. In the formation of V_{Ti} and V_C, the strong Ti–C covalent bond is broken; this is the driving force behind the decrease in the lattice constant in the (0001) plane. In the formation of V_A, the bonds between Al/Si atoms and the surrounding atoms are broken. According to our previous

analysis of diffusion barriers, the interactions between the Al/Si layer and the two neighboring Ti layers are stronger than the in-plane interactions for V_A. The formation of V_A therefore contracts the materials along the [0001] direction.

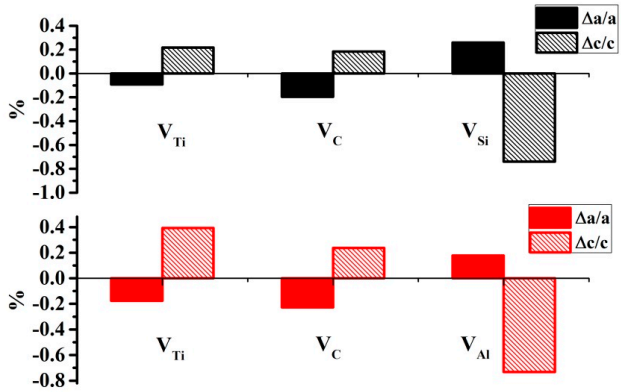

Figure 7. Lattice constant changes for Ti_3SiC_2 (black bar) and Ti_3AlC_2 (red bar) with respect to three types of on-site vacancies at a concentration of 12.5%. The difference between the results for Ti(a) and Ti(b) is very small, therefore the values are averaged as V_{Ti} for clarity.

To verify this conclusion, the interactions between atoms in Ti_3SiC_2 with vacancies were analyzed based on the deformation charge densities. As shown in Figure 8, unlike the electron density distributions in the configurations of V_{Ti} and V_C, there is an electron accumulation area around the two Ti atoms neighboring V_A. The electron accumulation of these two Ti atoms along the [0001] direction indicates that the interaction between them is enhanced by the Si vacancy. The effects of V_{Si} on the lattice constants are therefore different from those of V_{Ti} and V_C.

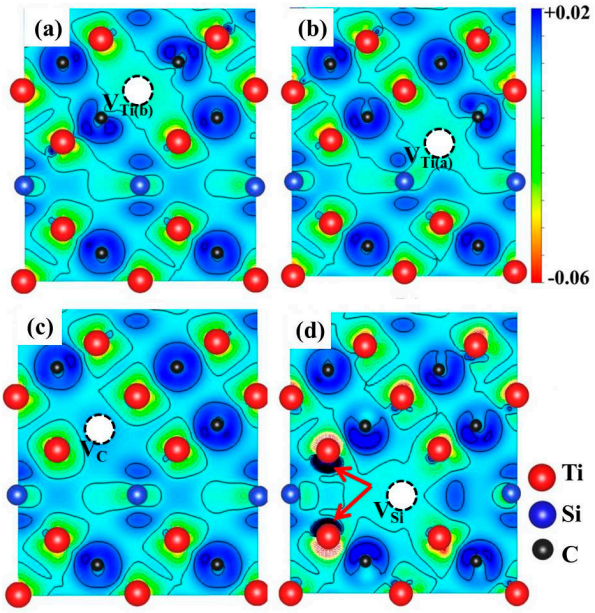

Figure 8. Deformation charge density (difference between crystal charge and atomic charge distribution) on (1, 1, $\bar{2}$, 0) plane of Ti_3SiC_2 with (**a**) $V_{Ti(b)}$; (**b**) $V_{Ti(a)}$; (**c**) V_C; and (**d**) V_{Si} vacancies. Contours added with intervals of 0.005 electrons/Bohr^3. Red and blue isosurfaces correspond to electron-depleted and electron-enriched zones, respectively. White circles indicate positions of vacancies. Electron accumulation areas around two Ti atoms neighboring V_A in (d) are indicated by red arrows.

4. Conclusions

In this study, the properties of vacancies in Ti_3AlC_2 and Ti_3SiC_2, which are two of the most widely studied MAX phases, were investigated using first-principles calculations. Our results show that an A-group element vacancy (V_A) has the lowest formation energy, therefore the vacancy–vacancy interactions, the effects of V_A on the lattice constants, and the charge redistribution of V_A were studied. The formation energy of V_{Al} is 0.9 eV lower than that of V_{Si}, indicating that an A-group element mono-vacancy is more easily formed in Ti_3AlC_2. Although the diffusion barriers for Ti_3SiC_2 and Ti_3AlC_2 are similar (~0.95 eV), the vacancy properties are different. Our results show that the vacancy–vacancy interaction is attractive in Ti_3AlC_2 but repulsive in Ti_3SiC_2. The vacancies therefore tend to disperse in Ti_3SiC_2 but are accommodated in Ti_3AlC_2. Based on these results, we conclude that Ti_3SiC_2 should be more stable than Ti_3AlC_2 in a corrosive environment. The introduction of V_{Ti} and V_C vacancies causes the lattice constant c along the [0001] direction to increase for both Ti_3SiC_2 and Ti_3AlC_2. The changes in the lattice constants caused by V_A are opposite. The effect of V_A on the lattice constants is explained by enhanced interactions of nearby Ti layers.

Acknowledgments: This work was supported by the Program of International S&T Cooperation (Grant No. 2014DFG60230), National Natural Science Foundation of China (Nos. 11605273, 91326105, U1404111, 11504089, 21501189, 21676291), the Shanghai Municipal Science and Technology Commission (16ZR1443100), the Strategic Priority Research Program of the Chinese Academy of Sciences (XDA02040104). We also thank the Supercomputing Center of Chinese Academy of Sciences (SCCAS) and the Shanghai Supercomputing Center for computer resources.

Author Contributions: Han Han and Ping Huai conceived and designed the whole study. Hui Wang, Han Han, Yu-Yang Hou, and Jun Tang performed DFT calculations. Chang-Ying Wang, Jian-Xing Dai, Cui-Lan Ren, and Wei Zhang analyzed the data. Han Han and Hui Wang co-wrote the manuscript. Ping Huai and Gen Yin helped with correction, modification, and revision of the manuscript.

Conflicts of Interest: The authors declare no conflict of interest.

References

1. Ghidiu, M.; Lukatskaya, M.R.; Zhao, M.-Q.; Gogotsi, Y.; Barsoum, M.W. Conductive two-dimensional titanium carbide 'clay' with high volumetric capacitance. *Nature* **2014**, *516*, 78–81. [CrossRef] [PubMed]
2. Naguib, M.; Mochalin, V.N.; Barsoum, M.W.; Gogotsi, Y. 25th Anniversary Article: Mxenes: A New Family of Two-Dimensional Materials. *Adv. Mater.* **2014**, *26*, 992–1005. [CrossRef] [PubMed]
3. Radovic, M.; Barsoum, M.W. Max phases: Bridging the gap between metals and ceramics. *Am. Ceram. Soc. Bull.* **2013**, *92*, 20–27.
4. Barsoum, M.W.; El-Raghy, T. Synthesis and Characterization of a Remarkable Ceramic: Ti_3SiC_2. *J. Am. Ceram. Soc.* **1996**, *79*, 1953–1956. [CrossRef]
5. Barsoum, M.W. The $M_{N+1}AX_N$ Phases: A New Class of Solids: Thermodynamically stable nanolaminates. *Prog. Solid State Chem.* **2000**, *28*, 201–281. [CrossRef]
6. Barsoum, M.W.; El-Raghy, T.; Rawn, C.J.; Porter, W.D.; Wang, H.; Payzant, E.A.; Hubbard, C.R. Thermal properties of Ti_3SiC_2. *J. Phys. Chem. Solids* **1999**, *60*, 429–439. [CrossRef]
7. Kisi, E.H.; Crossley, J.A.A.; Myhra, S.; Barsoum, M.W. Structure and Crystal Chemistry of Ti_3SiC_2. *J. Phys. Chem. Solids* **1998**, *59*, 1437–1443. [CrossRef]
8. Zhang, H.; Bao, Y.; Zhou, Y. Current Status in Layered Ternary Carbide Ti_3SiC_2, a Review. *J. Mater. Sci. Technol.* **2009**, *25*, 1–38.
9. Farber, L.; Levin, I.; Barsoum, M.W.; El-Raghy, T.; Tzenov, T. High-resolution transmission electron microscopy of some $Ti_{n+1}AX_n$ compounds (n = 1, 2; A = Al or Si; X = C or N). *J. Appl. Phys.* **1999**, *86*, 2540–2543. [CrossRef]
10. Wang, J.-Y.; Zhou, Y.-C. Polymorphism of Ti_3SiC_2 ceramic: First-principles investigations. *Phys. Rev. B* **2004**, *69*, 144108. [CrossRef]
11. Nappé, J.C.; Monnet, I.; Grosseau, P.; Audubert, F.; Guilhot, B.; Beauvy, M.; Benabdesselam, M.; Thomé, L. Structural changes induced by heavy ion irradiation in titanium silicon carbide. *J. Nucl. Mater.* **2011**, *409*, 53–61. [CrossRef]

12. Liu, X.M.; Le Flem, M.; Béchade, J.L.; Monnet, I. Nanoindentation investigation of heavy ion irradiated $Ti_3(Si,Al)C_2$. *J. Nucl. Mater.* **2010**, *401*, 149–153. [CrossRef]
13. Whittle, K.R.; Blackford, M.G.; Aughterson, R.D.; Moricca, S.; Lumpkin, G.R.; Riley, D.P.; Zaluzec, N.J. Radiation tolerance of $M_{n+1}AX_n$ phases, Ti_3AlC_2 and Ti_3SiC_2. *Acta Mater.* **2010**, *58*, 4362–4368. [CrossRef]
14. Hoffman, E.N.; Vinson, D.W.; Sindelar, R.L.; Tallman, D.J.; Kohse, G.; Barsoum, M.W. MAX phase carbides and nitrides: Properties for future nuclear power plant in-core applications and neutron transmutation analysis. *Nucl. Eng. Des.* **2012**, *244*, 17–24. [CrossRef]
15. Wang, J.; Zhou, Y.; Liao, T.; Zhang, J.; Lin, Z. A first-principles investigation of the phase stability of Ti_2AlC with Al vacancies. *Scr. Mater.* **2008**, *58*, 227–230. [CrossRef]
16. Liao, T.; Wang, J.; Zhou, Y. Ab initio modeling of the formation and migration of monovacancies in Ti_2AlC. *Scr. Mater.* **2008**, *59*, 854–857. [CrossRef]
17. Liao, T.; Wang, J.; Zhou, Y. First-principles investigation of intrinsic defects and (N, O) impurity atom stimulated Al vacancy in Ti_2AlC. *Appl. Phys. Lett.* **2008**, *93*, 261911. [CrossRef]
18. Music, D.; Ahuja, R.; Schneider, J.M. Theoretical study of nitrogen vacancies in Ti_4AlN_3. *Appl. Phys. Lett.* **2005**, *86*, 031911. [CrossRef]
19. Jie, T.; Han, H.; Darshana, W.; Wenguan, L.; Mingwen, Z.; Ping, H. A comparative first-principles study of the electronic, mechanical, defect and acoustic properties of Ti_2AlC and Ti_3AlC. *J. Phys. D Appl. Phys.* **2014**, *47*, 215301.
20. Du, Y.L.; Sun, Z.M.; Hashimoto, H.; Tian, W.B. First-Principles Study of Carbon Vacancy in Ta_4AlC_3. *Mater. Trans.* **2008**, *49*, 1934–1936. [CrossRef]
21. Han, H.; Wickramaratne, D.; Huang, Q.; Dai, J.; Li, T.; Wang, H.; Zhang, W.; Huai, P. A first-principles study on the defective properties of MAX phase Cr_2AlC: The magnetic ordering and strong correlation effect. *RSC Adv.* **2016**, *6*, 84262–84268. [CrossRef]
22. Medvedeva, N.I.; Novikov, D.L.; Ivanovsky, A.L.; Kuznetsov, M.V.; Freeman, A.J. Electronic properties of Ti_3SiC_2-based solid solutions. *Phys. Rev. B* **1998**, *58*, 16042–16050. [CrossRef]
23. Zhao, S.; Xue, J.; Wang, Y.; Huang, Q. Ab initio study of irradiation tolerance for different $M_{n+1}AX_n$ phases: Ti_3SiC_2 and Ti_3AlC_2. *J. Appl. Phys.* **2014**, *115*, 023503. [CrossRef]
24. Liu, X.; Le Flem, M.; Béchade, J.-L.; Onimus, F.; Cozzika, T.; Monnet, I. XRD investigation of ion irradiated $Ti_3Si_{0.90}Al_{0.10}C_2$. *Nucl. Instrum. Methods B* **2010**, *268*, 506–512. [CrossRef]
25. Nappé, J.C.; Monnet, I.; Audubert, F.; Grosseau, P.; Beauvy, M.; Benabdesselam, M. Formation of nanosized hills on Ti_3SiC_2 oxide layer irradiated with swift heavy ions. *Nucl. Instrum. Methods B* **2012**, *270*, 36–43. [CrossRef]
26. Marion, L.F.; Monnet, I. Saturation of irradiation damage in $(Ti,Zr)_3(Si,Al)C_2$ compounds. *J. Nucl. Mater.* **2013**, *433*, 534–537. [CrossRef]
27. Song, P.; Sun, J.; Wang, Z.; Cui, M.; Shen, T.; Li, Y.; Pang, L.; Zhu, Y.; Huang, Q.; Lü, J. Irradiation resistance properties studies on helium ions irradiated MAX phase Ti_3AlC_2. *Nucl. Instrum. Methods B* **2014**, *326*, 332–336. [CrossRef]
28. Zhang, L.; Qi, Q.; Shi, L.Q.; O'Connor, D.J.; King, B.V.; Kisi, E.H.; Venkatachalam, D.K. Damage tolerance of Ti_3SiC_2 to high energy iodine irradiation. *Appl. Surf. Sci.* **2012**, *258*, 6281–6287. [CrossRef]
29. Huang, Q.; Liu, R.; Lei, G.; Huang, H.; Li, J.; He, S.; Li, D.; Yan, L.; Zhou, J.; Huang, Q. Irradiation resistance of MAX phases Ti_3SiC_2 and Ti_3AlC_2: Characterization and comparison. *J. Nucl. Mater.* **2015**, *465*, 640–647. [CrossRef]
30. Wang, C.; Yang, T.; Kong, S.; Xiao, J.; Xue, J.; Wang, Q.; Hu, C.; Huang, Q.; Wang, Y. Effects of He irradiation on Ti_3AlC_2: Damage evolution and behavior of He bubbles. *J. Nucl. Mater.* **2013**, *440*, 606–611. [CrossRef]
31. Yang, T.; Wang, C.; Taylor, C.A.; Huang, X.; Huang, Q.; Li, F.; Shen, L.; Zhou, X.; Xue, J.; Yan, S.; et al. The structural transitions of Ti_3AlC_2 induced by ion irradiation. *Acta Mater.* **2014**, *65*, 351–359. [CrossRef]
32. Kresse, G.; Furthmüller, J. Efficiency of ab-initio total energy calculations for metals and semiconductors using a plane-wave basis set. *Comp. Mater. Sci.* **1996**, *6*, 15–50. [CrossRef]
33. Kresse, G.; Furthmüller, J. Efficient iterative schemes for ab initio total-energy calculations using a plane-wave basis set. *Phys. Rev. B* **1996**, *54*, 11169–11186. [CrossRef]
34. Blöchl, P.E. Projector augmented-wave method. *Phys. Rev. B* **1994**, *50*, 17953–17979. [CrossRef]
35. Perdew, J.P.; Wang, Y. Accurate and simple analytic representation of the electron-gas correlation energy. *Phys. Rev. B* **1992**, *45*, 13244–13249. [CrossRef]

36. Perdew, J.P.; Burke, K.; Ernzerhof, M. Generalized Gradient Approximation Made Simple. *Phys. Rev. Lett.* **1996**, *77*, 3865–3868. [CrossRef] [PubMed]
37. Henkelman, G.; Arnaldsson, A.; Jónsson, H. A fast and robust algorithm for bader decomposition of charge density. *Comp. Mater. Sci.* **2006**, *36*, 354–360. [CrossRef]
38. Huang, Q.; Han, H.; Liu, R.; Lei, G.; Yan, L.; Zhou, J.; Huang, Q. Saturation of ion irradiation effects in MAX phase Cr_2AlC. *Acta Mater.* **2016**, *110*, 1–7. [CrossRef]
39. Pack, J.D.; Monkhorst, H.J. "Special points for Brillouin-zone integrations"—A reply. *Phys. Rev. B* **1977**, *16*, 1748–1749. [CrossRef]
40. Henkelman, G.; Uberuaga, B.P.; Jónsson, H. A climbing image nudged elastic band method for finding saddle points and minimum energy paths. *J. Chem. Phys.* **2000**, *113*, 9901–9904. [CrossRef]
41. Henkelman, G.; Jónsson, H. Improved tangent estimate in the nudged elastic band method for finding minimum energy paths and saddle points. *J. Chem. Phys.* **2000**, *113*, 9978–9985. [CrossRef]
42. Onodera, A.; Hirano, H.; Yuasa, T.; Gao, N.F.; Miyamoto, Y. Static compression of Ti_3SiC_2 to 61 GPa. *Appl. Phys. Lett.* **1999**, *74*, 3782–3784. [CrossRef]
43. Hill, R. The Elastic Behaviour of a Crystalline Aggregate. *Proc. Phys. Soc. A* **1952**, *65*, 349. [CrossRef]
44. Han, H.; Cheng, C.; Xiong, X.-G.; Su, J.; Dai, J.-X.; Wang, H.; Yin, G.; Huai, P. Piezoelectric, Mechanical and Acoustic Properties of $KNaNbOF_5$ from First-Principles Calculations. *Materials* **2015**, *8*, 8578–8589. [CrossRef]
45. Han, H.; Yin, G.; Wickramaratne, D. A first-principles investigation of the electronic, elastic, piezoelectric and acoustic properties of $K_3B_6O_{10}Cl$. *Comput. Mater. Sci.* **2013**, *69*, 81–86. [CrossRef]
46. Pietzka, M.A.; Schuster, J.C. Summary of Constitutional Data on the Aluminum-Carbon-Titanium System. *J. Phase Equilib.* **1994**, *15*, 392–400. [CrossRef]
47. Kornblit, L.; Pelleg, J.; Rabinovitch, A. Self-diffusion calculation for fcc metals. *Phys. Rev. B* **1977**, *16*, 1164–1167. [CrossRef]
48. García Ortega, M.; Ramos de Debiaggi, S.; Monti, A. Self-Diffusion in FCC Metals: Static and Dynamic Simulations in Aluminium and Nickel. *Phys. Stat. Sol. (b)* **2002**, *234*, 506–521. [CrossRef]
49. Atkinson, A.; Taylor, R.I. The diffusion of Ni in the bulk and along dislocations in NiO single crystals. *Philos. Mag. A* **1979**, *39*, 581–595. [CrossRef]
50. Debiaggi, S.; Decorte, P.; Monti, A. Diffusion by Vacancy Mechanism in Ni, Al, and Ni_3Al: Calculation Based on Many-Body Potentials. *Phys. Stat. Sol. (b)* **1996**, *195*, 37–54. [CrossRef]